

External cavity semiconductor laser model for the strong feedback regime

L. RAMUNNO*† and J. E. SIPE

Department of Physics, University of Toronto, Toronto, Canada

(Received 20 April 2004; in final form 25 October 2004)

We present a formalism describing the dynamics of a semiconductor diode and apply it to the study of the dynamics of external cavity lasers within the strong regime. The formalism is based upon the usual travelling wave phenomenological model for the field and carriers within the semiconductor gain medium. Since the non-radiative recombination time of the carriers is typically much longer than the diode round trip time, we use a multiple scales analysis to obtain a model much simpler in form than the travelling wave model, but as accurate, without assuming that the gain within the diode is uniform. We apply this model to the external cavity laser. Rather than including multiple external cavity reflections explicitly, we include all external cavity reflections through the introduction of a single additional feedback parameter and one extra term in the field equation. In the limit of a single external cavity reflection, our field equation reduces to a form of the well-known Lang–Kobayashi equation that describes very weak external feedback. For strong feedback, we examine both the steady state and dynamical laser properties such as small signal response and large signal current modulation.

1. Introduction

Semiconductor laser diodes are the active elements of many multi-component systems, such as external cavity semiconductor lasers, in both continuous-wave (CW) [1–3] and directly-modulated operation [4–6]. For most applications, a phenomenological model employing slowly-varying envelope functions has been shown to describe the dynamics of the field within the diode gain medium appropriately, giving reasonable agreement with experiment [7–9]. A standard description consists of a set of coupled nonlinear partial differential equations (PDEs) for the field and electron–hole (carrier) density within the active layer that must be solved numerically [8, 10]. The numerical solution of these equations, however, can be quite cumbersome, especially when elements external to the diode itself are included in the system of interest. An example is external cavity semiconductor lasers, where often only a single external cavity reflection can be reasonably included in the calculation [11]. Further, it is difficult to gain an understanding of the underlying physics through purely numerical methods. The usual approximation

*Corresponding author. Email: lora.ramunno@science.uottawa.ca

†Current address: Department of Physics, University of Ottawa, Ottawa, Canada.

made to obtain a more simple form is to assume that the carrier density and gain are uniform along the length of the diode. Then the dynamics are described by a set of rate equations for the photon and carrier densities, and for the phase of the electric field [7, 9, 12]. For some regions of parameter space this approximation is reasonable, but for many regimes of interest it is not [13].

The goal of this paper is two-fold. First we introduce a new formalism describing the dynamics of the semiconductor gain medium that is as accurate as the usual nonlinear coupled PDE model, but no more complicated in form than usual rate equation models. It is easily applied in the study of more complicated physical systems like external cavity lasers, and can be used to describe large signal current modulation. Unlike previous work [14], this diode model is able to describe dynamics on the time scale of the round trip time of light within the diode itself. Our second aim is to present an application of this diode formalism to the study of the external cavity semiconductor laser, with particular focus on very strong feedback and direct current modulation, as typical of current lasers of interest [1–6, 15]. Although we consider in this paper only non-dispersive feedback, the diode formalism is general enough to describe arbitrary systems incorporating semiconductor diodes. This includes lasers with filtered optical feedback, which have been of recent interest [16–19]. The importance of this type of laser stems from the frequency selective feedback which may be tailored to give some control over the complex nonlinear dynamics of semiconductor lasers, as has been shown by recent experimental and theoretical work [20].

The diode formalism is presented in section 2. Exploiting the time scale difference between the relaxation time of the carrier density and the round trip time of light within the diode, the latter typically much faster than the former, we perform a multiple scales analysis [14, 21] of the PDE model. This difference in time scales has also been noted and used non-rigorously in other works [12, 22], and is discussed in appendix A. It follows from our analysis, not surprisingly, that to zeroth order the dynamics of the carrier density occur on a time scale that is slower than the diode round trip time, while the field envelope function dynamics generally do not. The resulting equations take a simple form, where the dynamics within the diode active region are described accurately by a single ordinary differential equation for the total carrier density within the diode in terms of the fields at the diode boundaries—a form similar to that of previous work [14]—and time-delay relations between the boundary fields describing propagation and amplification through the diode. The complicated dynamics within the diode need not be calculated, even for steady state; the diode can be treated effectively as a ‘black box’ even though the diode dynamics are nonlinear. In addition, the model is not restricted to describing the dynamics of a single longitudinal mode.

This formalism describes the diode as a simple amplifier. It is easily extended, however, to the study of composite laser systems; one need only supply appropriate boundary conditions relating the input and output fields at both diode facets. We do this in section 3 in our study of non-dispersive external cavity diode lasers. Using the formalism of section 2, it is quite natural to incorporate both multiple solitary diode longitudinal modes [11, 23] and an infinite number of external cavity reflections—but in a very simple way—in order to derive a generalized Lang–Kobayashi (LK) equation which resembles the standard LK equation [12, 24] in the limit of a single external cavity reflection. The generalized model is especially useful for describing external cavity lasers operating within the strong feedback

regime (corresponding approximately to ‘Regime V’ [25]), though it can be used in any regime. We show in 3.1, with details deferred to appendix B, that our model is equivalent to other multiple external cavity reflection models wherein each external reflection is accounted for explicitly [12, 26–29]. Our description, however, does not require that the field be known at all past integer multiples of the external cavity round trip times, and it does not require that additional approximations be made to achieve a simpler form [30]. In fact, all external cavity reflections (after the first) are incorporated easily by introducing one additional feedback parameter and one extra term in the field equation. And this is accomplished not only for steady state mode calculations, which we show in 3.2 reproduce known results [22, 30, 31], but for a general dynamical description capable of describing arbitrary current modulation. In 3.3 we present this dynamical description, applying it first to examine the stability properties from the linearized laser equations, then to obtain numerical solutions for large signal current modulation for a laser with strong external feedback.

Conclusions are given in section 4.

2. Semiconductor diode model

We begin with the usual coupled nonlinear phenomenological equations for the electron–hole (carrier) density within the semiconductor gain medium $N(z, t)$, and for the counter-propagating electric field envelope functions $E_{\pm}(z, t)$ defined by

$$E(z, t) = E_+(z, t) \exp(ikz) \exp(-i\omega t) + E_-(z, t) \exp(-ikz) \exp(-i\omega t) + c.c.,$$

where $E(z, t)$ is the field for a given transverse mode and z is the direction of propagation along the diode length. The carrier frequency is ω and its associated wavevector is $k \equiv n_g \omega / c$, where n_g is the background index of refraction of the unpumped gain medium and c is the speed of light in vacuum. The phenomenological equations are [10, 11, 14, 32–38]

$$\frac{\partial E_{\pm}}{\partial t} \pm v_g \frac{\partial E_{\pm}}{\partial z} = \frac{1}{2} \Gamma v_g a [(N - N_t) - i\beta_c N] E_{\pm}, \tag{1}$$

$$\frac{\partial N}{\partial t} = \frac{J}{ed} - \frac{N}{T_n} - v_g a (N - N_t) (S_+ + S_-), \tag{2}$$

where effective photon densities are defined by

$$S_{\pm}(z, t) = \frac{n_g^2}{2\pi\hbar\omega} |E_{\pm}(z, t)|^2,$$

where e is the charge of an electron and $J(t)$ is the current density, which must be supplied as a function of time. The phenomenological model parameters are defined in table 1, where typical values are listed. For simplicity, we neglect the effects of gain compression, but this can be easily generalized; in previous work [13], we have shown its inclusion provides only a very small correction to the large field and carrier density transients resulting from large signal current modulation. To complete the phenomenological description, (1) and (2) must be supplemented by appropriate

Table 1. Semiconductor diode parameters.

Parameter	Symbol	Value
Differential gain	a	$2.22 \times 10^{-16} \text{ cm}^2$
Linewidth enhancement factor	β_c	2
Transparency carrier density	N_t	$2.053 \times 10^{17} \text{ cm}^{-3}$
Carrier relaxation time	T_n	1 ns
Mode confinement factor	Γ	0.34
Effective waveguide thickness	d	0.15 μm
Background refractive index	n_g	3.7
Diode length	L_g	250 μm
Group velocity in diode	v_g	$\equiv c/n_g$
Round trip time in diode	T_g	$\equiv 2L_g/v_g$
Normalized transp. density	a_0	$\equiv 2L_g\Gamma a N_t$

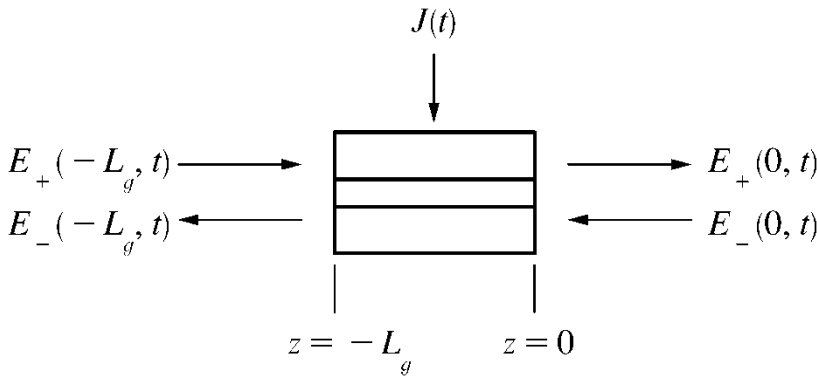


Figure 1. Schematic diagram of a semiconductor laser diode, with bias current density $J(t)$ and boundary fields $E_-(0, t), E_+(0, t)$ at the $z=0$ diode facet, and boundary fields $E_-(-L_g, t), E_+(-L_g, t)$ at the $z=-L_g$ diode facet.

boundary conditions for the electric field envelope functions at the diode facets, drawn schematically in figure 1. We set L_g as the length of the diode and, as indicated in figure 1, choose the diode boundaries to be located at $z = -L_g$ and $z = 0$. Since the ultimate purpose of the model we develop here is for use in the description of strongly dispersive feedback, we also neglect gain dispersion, although it can be included in a simple way by approximating the semiconductor gain curve by a quadratic function [11, 28].

To proceed with our multiple scales analysis, we rewrite (1) and (2) in dimensionless form, so the relative magnitudes of the terms become apparent. We define normalized time and length variables by

$$\hat{z} = z/(2L_g),$$

$$\hat{t} = t/T_g,$$

where $T_g \equiv 2L_g/v_g$ is the round trip time of light within the diode and v_g is the group velocity of the unpumped medium. The normalized round trip time is 1 in these new variables and the normalized diode length is 1/2; the diode facets are located at

$\hat{z} = -1/2$ and $\hat{z} = 0$. We define dimensionless versions of E_{\pm} , N , J in terms of these dimensionless variables \hat{z} , \hat{t} ,

$$e_{\pm}(\hat{z}, \hat{t}) = \left(\frac{\mu v_g a T_n n_g^2}{2\pi \hbar \omega} \right)^{1/2} E_{\pm}(z, t) \exp\left(\pm i \frac{\beta_c}{2} \Gamma a N_t z \right),$$

$$n(\hat{z}, \hat{t}) = 2L_g \Gamma a (N(z, t) - N_t),$$

$$j(\hat{t}) = 2L_g \Gamma a T_n \mu \left(\frac{J(t)}{ed} - \frac{N_t}{T_n} \right).$$

The steady state solutions of e_{\pm} , n , j have a magnitude of order unity for typical systems and operating regimes. We have defined a small parameter μ by

$$\mu = (T_g/T_n)^{1/2},$$

where typically $\mu \ll 1$ since $T_g \approx 6$ ps and the carrier density relaxation time $T_n \approx 1$ ns. The phenomenological equations (1) and (2) become

$$\frac{\partial e_{\pm}(z, t)}{\partial t} \pm \frac{\partial e_{\pm}(z, t)}{\partial z} = \frac{1}{2} (1 - i\beta_c) n(z, t) e_{\pm}(z, t), \tag{3}$$

$$\frac{1}{\mu} \frac{\partial n(z, t)}{\partial t} = j(t) - \mu n(z, t) - n(z, t) (|e_+(z, t)|^2 + |e_-(z, t)|^2), \tag{4}$$

where we have dropped the ‘hats’ on \hat{z} and \hat{t} for convenience.

We perform a standard multiple scales analysis [14, 21] by seeking solutions of (3) and (4) of the form

$$e_{\pm}(z, t) = e_{\pm}^{(0)}(z; t_0, t_1, \dots) + \mu e_{\pm}^{(1)}(z; t_0, t_1, \dots) + \dots, \tag{5}$$

$$n(z, t) = n^{(0)}(z; t_0, t_1, \dots) + \mu n^{(1)}(z; t_0, t_1, \dots) + \dots, \tag{6}$$

where we introduce independent time variables

$$t_m \equiv \mu^m t \tag{7}$$

for $m = 0, 1, 2, \dots$, in terms of the small parameter μ . The magnitudes of each function $e_{\pm}^{(p)}$ and $n^{(p)}$ are assumed to be of order unity or smaller, and they are assumed to vary significantly only as each of their temporal arguments t_m varies from 0 to 1 (or possibly greater than 1). As the fastest time scale t_0 varies from 0 to 1, real time varies from 0 to T_g , so that dynamics on the order of the diode round trip time are captured in the functions $e_{\pm}^{(p)}$ and $n^{(p)}$ *only* by their dependence on time variable t_0 . As the slower time scale t_1 varies from 0 to 1, real time varies from 0 to $(T_n T_g)^{1/2} \approx 80$ ps. This is typically of the order of the rate of change of any current modulation in directly-modulated systems. Thus the normalized current density above transparency, which in general we would write as $j(t_0, t_1, \dots)$, is typically independent of t_0 ; this is what we assume below. The slow non-radiative relaxation

of the carriers is captured in the time scale t_2 , which varies from 0 to 1 as real time varies from 0 to T_n . From (7), the partial time derivative is

$$\frac{\partial}{\partial t} = \frac{\partial}{\partial t_0} + \mu \frac{\partial}{\partial t_1} + \mu^2 \frac{\partial}{\partial t_2} + \dots \tag{8}$$

Inserting (5), (6) and (8) into (3) and (4), we collect terms multiplied by different powers of μ ; by requiring that the resulting equations are satisfied to higher and higher order in μ , we expect an asymptotically better description. We have, to order $1/\mu$,

$$\frac{\partial}{\partial t_0} n^{(0)}(z; t_0, t_1, \dots) = 0. \tag{9}$$

This implies that $n^{(0)}$ is independent of the fastest time variable t_0 . Then to zeroth order, the carrier density does not vary significantly on the time scale of the diode round trip time, T_g ; its fastest variation occurs on the time scale of t_1 , or possibly slower. As we discuss in appendix A, this slow time variation of the carrier density appears in the derivations of rate equations for both a standard solitary diode laser and an external cavity laser, including a derivation of the Lang–Kobayashi equation. In most of this previous work, this assumption is not stated explicitly, but is an implicit consequence of the approximations that are made in order to obtain the final form of the field equations.

We collect the zeroth-order terms to obtain

$$\left(\frac{\partial}{\partial t_0} \pm \frac{\partial}{\partial z} \right) e_{\pm}^{(0)}(z; t_0, t_1) = \frac{1}{2} (1 - i\beta_c) n^{(0)}(z; t_1) e_{\pm}^{(0)}(z; t_0, t_1) \tag{10}$$

and

$$\begin{aligned} \frac{\partial}{\partial t_0} n^{(1)}(z; t_0, t_1) + \frac{\partial}{\partial t_1} n^{(0)}(z; t_1) = j(t_1) - n^{(0)}(z; t_1) \\ \times \left(|e_+^{(0)}(z; t_0, t_1)|^2 + |e_-^{(0)}(z; t_0, t_1)|^2 \right). \end{aligned} \tag{11}$$

Since we consider here only the equations up to order μ^0 , we explicitly indicate only the t_0 and t_1 variables. To derive a more useful version of (10), we first transform it to the Fourier domain to obtain

$$\frac{\partial}{\partial z} \tilde{e}_{\pm}^{(0)}(z; \Omega_0, t_1) = \pm \left[\frac{1}{2} (1 - i\beta_c) n^{(0)}(z; t_1) + i\Omega_0 \right] \tilde{e}_{\pm}^{(0)}(z; \Omega_0, t_1),$$

where $\tilde{e}_{\pm}^{(0)}(z; \Omega_0, t_1)$ is the Fourier transform of $e_{\pm}^{(0)}(z; t_0, t_1)$ in the t_0 variable; this equation has a simple form since $n^{(0)}(z; t_1)$ is independent of t_0 . We solve this differential equation in z by using the integrating factor

$$\exp \left[\mp \int^z \frac{1}{2} (1 - i\beta_c) n^{(0)}(z'; t_1) + i\Omega_0 \right] dz',$$

and integrate the resulting equation from z_2 to z_1 to obtain

$$\tilde{e}_{\pm}^{(0)}(z_1; \Omega_0, t_1) = \exp\left[\pm \frac{1}{2}(1 - i\beta_c) \int_{z_2}^{z_1} n^{(0)}(z; t_1) dz \pm i\Omega_0(z_1 - z_2)\right] \tilde{e}_{\pm}^{(0)}(z_2; \Omega_0, t_1).$$

Finally, putting $z_1 = 0$ and $z_2 = -1/2$ and transforming back to the t_0 time domain, we obtain a time-delayed relation between the fields at the diode boundaries,

$$e_{\pm}^{(0)}(0; t_0, t_1) = \exp\left[\pm \frac{1}{4}(1 - i\beta_c) \sigma^{(0)}(t_1)\right] e_{\pm}^{(0)}(-1/2; t_0 \mp 1/2, t_1). \tag{12}$$

This describes the effects of gain and propagation on the forward and backward propagating fields due to a single pass through the semiconductor diode. A (normalized) average carrier density above transparency within the diode is defined as

$$\sigma^{(0)}(t_1) \equiv 2 \int_{-1/2}^0 n^{(0)}(z; t_1) dz.$$

Combining (12) with appropriate boundary conditions for the fields at the diode facets, a single delay equation can be obtained in terms of one of these boundary fields. For a particular system, this single delay equation can be directly compared to the corresponding field equation of a standard rate equation model by first making a Taylor expansion of the delayed field in (12), and then keeping only the first order in the expansion to obtain a first-order time derivative of the field. We do this in section 3 for the external cavity laser and show how, in the limit of a single external cavity reflection, we obtain an equation for $e_{+}^{(0)}(0; t_0, t_1)$ that resembles the Lang–Kobayashi equation.

We seek from (11) an equation describing the t_1 time dependence of $\sigma^{(0)}$. It turns out to be useful, and valid in the description of a large class of systems, to assume the following form for the electric field envelope functions

$$e_{\pm}^{(0)}(z; t_0, t_1) = \sum_{m=-\infty}^{\infty} e_{\pm(m)}^{(0)}(z; t_1) \exp\left(-i \frac{2\pi}{\tau_p} m t_0\right). \tag{13}$$

That is, the field is assumed periodic in the fastest time scale t_0 with some period τ_p , but can have arbitrary time dependence in all other time scales. The period τ_p is chosen according to the boundary conditions of the system under consideration; as long as $\tau_p \ll 1/\mu$ there is no overlap between the t_0 and t_1 time scales. For example, to describe systems in which there is a significant reflectivity at each of the diode facets, it is most relevant to set $\tau_p = 1$, in recognition of the resonance condition formed by the two diode facets. In the case of an anti-reflection coated diode coupled to an external cavity, however, it makes more physical sense to choose τ_p to be the round trip time of the combined laser cavity. The form (13) essentially Fourier-decomposes the field into the multiple longitudinal modes of the relevant resonant cavity. The coefficients (or envelope functions) of these longitudinal modes, $e_{\pm(m)}^{(0)}(z; t_1)$, have arbitrary spatial dependence, but a

time dependence that is assumed to vary more slowly than T_g ; we later verify that this assumption is self-consistent. Using (13), (10) and (11) become

$$\frac{\partial}{\partial z} e_{\pm(m)}^{(0)}(z; t_1) = \pm \left(\frac{1 - i\beta_c}{2} n^{(0)}(z; t_1) + i \frac{2\pi}{\tau_p} m \right) e_{\pm(m)}^{(0)}(z; t_1), \quad (14)$$

$$\frac{\partial}{\partial t_1} n^{(0)}(z; t_1) = j(t_1) - n^{(0)}(z; t_1) \sum_m \left(|e_{+(m)}^{(0)}(z; t_1)|^2 + |e_{-(m)}^{(0)}(z; t_1)|^2 \right), \quad (15)$$

where to obtain (15) we isolated the secular pieces of (11); the non-secular pieces lead to an equation that describes the time evolution of the Fourier components of $n^{(1)}$. Using (14) to rewrite (15), we obtain

$$\frac{\partial}{\partial t_1} n^{(0)}(z; t_1) = j(t_1) - \frac{\partial}{\partial z} \sum_m \left(|e_{+(m)}^{(0)}(z; t_1)|^2 - |e_{-(m)}^{(0)}(z; t_1)|^2 \right). \quad (16)$$

Integrating (14) and (16) in z , from $z = -1/2$ to 0 , we obtain

$$e_{\pm(m)}^{(0)}(0; t_1) = \exp \left[\pm \frac{1}{4} (1 - i\beta_c) \sigma^{(0)}(t_1) \right] \exp(\pm i\pi m / \tau_p) e_{\pm(m)}^{(0)}(-1/2; t_1), \quad (17)$$

$$\begin{aligned} \frac{\partial}{\partial t_1} \sigma^{(0)}(t_1) = j(t_1) - 2 \sum_m \left(|e_{+(m)}^{(0)}(0; t_1)|^2 - |e_{-(m)}^{(0)}(0; t_1)|^2 \right. \\ \left. - |e_{+(m)}^{(0)}(-1/2; t_1)|^2 + |e_{-(m)}^{(0)}(-1/2; t_1)|^2 \right). \end{aligned} \quad (18)$$

Our model is now in a form that allows the incorporation of arbitrary boundary conditions, since the equations (17) and (18) contain only fields at the diode boundaries. It is thus straightforward to obtain dynamical equations for systems comprised of a diode coupled to external elements, such as the external cavity laser. With appropriate boundary conditions, equations for one set of the boundary fields, say $e_{+(m)}^{(0)}(0; t_1)$, can be obtained from (17), and these describe the t_1 time evolution for each of the corresponding longitudinal modes labelled by m . Applying the boundary conditions and (17) to (18), then it too can be rewritten in terms of the same set of boundary fields, giving a closed set of equations for $\sigma^{(0)}(t_1)$ and, say, $e_{+(m)}^{(0)}(0; t_1)$. To solve this numerically, it is also necessary to specify both the initial conditions and the (normalized) current density j as a function of time. The dynamics can thus be determined without having to solve for the fields and carrier density at each point along the diode—necessary in the direct application of (1) and (2)—yet without assuming uniform gain along the length of the diode. Further, it is much simpler to gain an understanding of the underlying physics of a particular composite system using (17) and (18) than the original equations (1) and (2). We turn now to an application of (17) and (18) to the study of semiconductor lasers with non-dispersive external feedback.

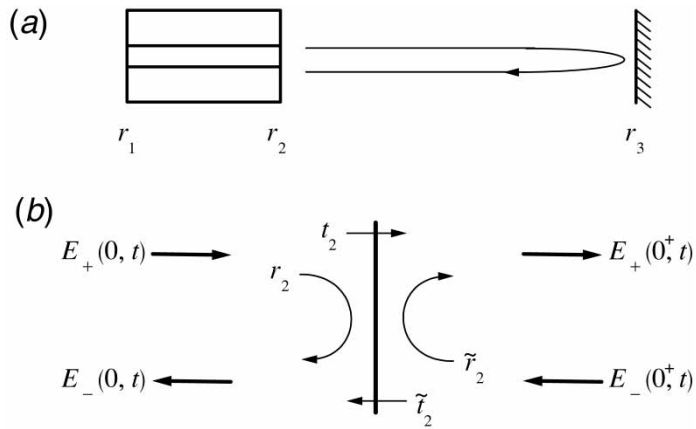


Figure 2. (a) Schematic diagram of an external cavity semiconductor laser and (b) the transfer region at the $z=0$ diode facet.

3. Diode with external feedback

In this section, we use the diode model of section 2 to describe external cavity semiconductor lasers, as sketched in figure 2(a). Our aims are to confirm the consistency of the diode model, compare our results with previous work, and present large signal modulation results for strong external feedback. In 3.1, we obtain a general equation for the field using both the time-delay multiple scales equation (12) and boundary conditions for the diode and external mirror; an infinite number of external cavity reflections are automatically included via a transfer matrix for the facet at $z=0$. These reflections are incorporated within the formalism through the introduction of a single new feedback parameter, and one additional term in the field equation. In appendix B, we show this approach is equivalent to incorporating each external cavity reflection directly, a method commonly used in models that consider strong external feedback. In the limit of a single reflection, our time-delay field equation is reduced to a form of the Lang-Kobayashi (LK) equation. In 3.2, we find the CW spectrum of the external cavity laser for both multiple and single reflection models. Based on the qualitative features of this CW spectrum, we make an appropriate choice for the quantity τ_p that appears in the Fourier decomposition (13), forming the basis of our dynamical model presented in 3.3. We perform a linear stability analysis and present two numerical examples for large signal current modulation for lasers with strong external feedback.

3.1 Field equation and the LK limit

To find a field equation for the external cavity laser illustrated in figure 2 (a) from (12), we must first determine the boundary conditions for the field envelope functions at both diode facets. For the facet located at $z = -L_g$ (the one not coupled to the external cavity) we have

$$E_+(-L_g, t) = r_1 \exp(2ikL_g) E_-(-L_g, t), \tag{19}$$

for complex reflection coefficient r_1 . We assume there is no external injection field, but this is easily generalized. The boundary condition for the fields at $z=0$ depends on the effective reflection and transmission coefficients of that diode facet and on the reflection coefficient of the external mirror, which we denote by r_3 . We assume r_3 is frequency independent and the external cavity is filled with a homogeneous, linear material. Denoting by $z=0^+$ the position just beyond the $z=0$ facet, the fields just outside the diode satisfy

$$E_-(0^+, t) = r_3 \exp(i\omega T_{\text{ext}}) E_+(0^+, t - T_{\text{ext}}), \quad (20)$$

where T_{ext} is the round trip time in the external cavity and where r_3 is complex. The fields at $z=0$ and $z=0^+$ are related via a transfer matrix,

$$\begin{aligned} E_-(0, t) &= r_2 E_+(0, t) + \tilde{t}_2 E_-(0^+, t), \\ E_+(0^+, t) &= t_2 E_+(0, t) + \tilde{r}_2 E_-(0^+, t). \end{aligned} \quad (21)$$

The coefficients r_2 , t_2 , \tilde{r}_2 and \tilde{t}_2 , labelled in figure 2(b), are in general complex. To obtain appropriate relations between these reflection and transmission coefficients, the details at the boundary need to be specified, i.e. whether the facet is bare or coated and the properties of any coating. Combining (20) and (21) we have [22]

$$\begin{aligned} E_-(0, t) &= r_2 E_+(0, t) + \tilde{r}_2 r_3 \exp(i\omega T_{\text{ext}}) E_-(0, t - T_{\text{ext}}) \\ &\quad + r_3 (\tilde{t}_2 t_2 - \tilde{r}_2 r_2) \exp(i\omega T_{\text{ext}}) E_+(0, t - T_{\text{ext}}). \end{aligned} \quad (22)$$

To make a connection to the literature, we show in appendix B that (22) can also be derived from the well-known boundary condition for external cavity lasers [12, 26–30],

$$E_-(0, t) = r_2 E_+(0, t) + \frac{\tilde{t}_2 t_2}{\tilde{r}_2} \sum_{n=1}^{\infty} (\tilde{r}_2 r_3)^n \exp(in\omega T_{\text{ext}}) E_+(0, t - nT_{\text{ext}}), \quad (23)$$

which explicitly contains an infinite number of external cavity reflections. While we do not use equation (23) in this paper, it is the boundary condition used most often in work that includes multiple external cavity reflections [12, 26–30], where usually further approximations are required in order to write the resulting laser field equation in a more practical form. Models including only a single external cavity reflection consider only the first term of the summation in (23).

We normalize the frequency variable and the external cavity round trip time with respect to T_g ,

$$\begin{aligned} \hat{\omega} &\equiv \omega T_g, \\ \tau &\equiv T_{\text{ext}}/T_g. \end{aligned}$$

Using $k = \omega/v_g$, (19) and (22) become, in normalized units,

$$\begin{aligned} e_+(-1/2, t) &= r_1 \exp[i(\hat{\omega} - \beta_c a_0/2)] e_-(-1/2, t), \\ e_-(0, t) &= r_2 e_+(0, t) + \tilde{r}_2 r_3 \exp(i\hat{\omega}\tau) e_-(0, t - \tau) \\ &\quad + r_3 (\tilde{t}_2 t_2 - \tilde{r}_2 r_2) \exp(i\hat{\omega}\tau) e_+(0, t - \tau), \end{aligned} \quad (24)$$

where a_0 is the normalized transparency density of the active medium, defined in table 1.

We must now choose appropriate boundary conditions for the multiple scales quantities. In general, these may be any that satisfy (24). The most straightforward procedure involves a multiple scales expansion of the fields in (24) in the same spirit as that in section 2, where collecting the terms of the same order in μ yields

$$e_+^{(p)}(-1/2; t_0, t_1) = r_1 \exp[i(\hat{\omega} - \beta_c a_0/2)] e_-^{(p)}(-1/2; t_0, t_1), \tag{25}$$

$$e_-^{(p)}(0; t_0, t_1) = r_2 e_+^{(p)}(0; t_0, t_1) + \tilde{r}_2 r_3 \exp(i\hat{\omega}\tau) e_-^{(p)}(0; t_0 - \tau, t_1 - \mu\tau) + r_3 \exp(i\hat{\omega}\tau) (\tilde{t}_2 t_2 - \tilde{r}_2 r_2) e_+^{(p)}(0; t_0 - \tau, t_1 - \mu\tau), \tag{26}$$

for $p = 0, 1, \dots$. For (26) to be consistent with the multiple scales assumptions—namely that the multiple scales functions vary significantly only as the t_p vary from 0 to 1 (or greater than 1)—then we should have $\tau \geq 1$ so the external cavity dynamics occur no faster than t_0 . This is typically the case for many external cavity lasers. For example, a 1 cm glass cavity (typical for fibre grating semiconductor lasers) corresponds to $\tau = 14$ and $\mu\tau = 1.2$. For a 1 m air-filled cavity, as used in many external cavity experiments with very weak feedback levels, then $\tau \approx 10^3$ and $\mu\tau \approx 80$.

We apply these boundary conditions to the time-delay field equation (12) to derive a field equation for one of the boundary fields, $e_+^{(0)}(0; t_0, t_1)$. Since in the remainder of the paper we use only the zeroth-order functions, we drop the superscript ‘(0)’ for convenience. Combining (25) for $p = 0$ with (12), we obtain

$$e_+(0; t_0 + 1, t_1) = \frac{1}{r_2} G(t_1) e_-(0; t_0, t_1),$$

where the gain due to a complete round trip through the diode is

$$G(t_1) \equiv r_1 r_2 \exp[i(\hat{\omega} - \beta_c a_0/2)] \exp\left[\frac{1}{2}(1 - i\beta_c)\sigma(t_1)\right]. \tag{27}$$

From (26) for $p = 0$, we obtain the general field equation for e_+ at $z = 0$

$$e_+(t_0 + 1, t_1) = G(t_1) e_+(t_0, t_1) + \alpha \exp(i\hat{\omega}\tau) \frac{G(t_1)}{G(t_1 - \mu\tau)} e_+(t_0 - \tau + 1, t_1 - \mu\tau) + (\gamma - \alpha) \exp(i\hat{\omega}\tau) G(t_1) e_+(t_0 - \tau, t_1 - \mu\tau), \tag{28}$$

where, again for convenience, we have omitted the explicit spatial dependence of e_+ , since in the rest of the paper we only consider the fields at $z = 0$. We have defined (complex) feedback parameters to be

$$\gamma \equiv r_3 \frac{\tilde{t}_2 t_2}{r_2},$$

$$\alpha \equiv \tilde{r}_2 r_3,$$

where γ corresponds to the usual feedback parameter of the LK model. Equation (28) is much easier to deal with than the usual equations describing multiple external cavity reflections. Here all reflections after the first are captured by a single additional feedback parameter α . We present later in 3.3 a complete dynamical description of the external cavity laser, where we use the field expansion (13) and the gain medium equations (14) and (16) to obtain a closed set of equations

for σ and the field modes $e_{+(m)}$. But first we examine only the field equation (28) to make a direct comparison with the LK model in the limit of a single external cavity reflection and, in 3.2, to find the CW frequency mode spectrum.

The form of the usual LK field equation is recovered from (28) for a single reflection by setting $\alpha = 0$, giving

$$\exp[-\log G(t_1)] \exp(\partial/\partial t_0) e_+(t_0, t_1) = e_+(t_0, t_1) + \gamma \exp(i\hat{\omega}\tau) e_+(t_0 - \tau, t_1 - \mu\tau),$$

where the logarithm is complex-valued. This corresponds to the form of ‘precursor to the LK equation’ (A 7) of appendix A, where we review a derivation of the LK field equation. Proceeding with our derivation here, we use

$$\exp(-\log G(t_1)) \exp(\partial/\partial t_0) = \exp(-\log G(t_1) + \partial/\partial t_0), \quad (29)$$

which is exact since

$$[G(t_1), \partial/\partial t_0] = 0, \quad (30)$$

the square brackets indicating a commutation operation. Expanding the resulting exponential function on the right-hand side of (29) and keeping only the first order, we obtain our version of the LK equation,

$$\frac{\partial}{\partial t_0} e_+(t_0, t_1) = [\log G(t_1)] e_+(t_0, t_1) + \gamma \exp(i\hat{\omega}\tau) e_+(t_0 - \tau, t_1 - \mu\tau). \quad (31)$$

Formula (30) is a consequence of the multiple scales analysis, since σ is independent of time t_0 ; the significance of (30) is apparent through a re-examination of the approximations made in the standard derivation of the LK rate equation with uniform gain, as discussed in appendix A. We show there that to obtain the final field rate equation from the ‘precursor’ (A 7), one needs a formula similar to (29), so it must be assumed that d/dt and the carrier density $N(t)$ commute. Then N should be, strictly speaking, time independent. Here this approximation need not be made for the derivation of (31), since (30) arises naturally from the multiple scales analysis, whose only assumption is that $T_n \gg T_g$. Furthermore, the carrier density here is allowed to have a slowly varying time dependence, through its dependence on time t_1 .

The inclusion of the external cavity reflections beyond the first, and thus the inclusion of terms containing α in (28), becomes important especially when the reflectivity at the $z=0$ diode facet is not small. For example, assuming that the $z=0$ facet of the diode is either bare or has a very thin dielectric coating, the boundary conditions at $z=0$ lead to $\tilde{t}_2 t_2 - \tilde{r}_2 r_2 = 1$ and $\tilde{r}_2 = -r_2$ for r_2 real. Then from the definitions of α and γ we have

$$\frac{|\alpha|}{|\gamma|} \equiv \frac{(r_2)^2}{1 - (r_2)^2}. \quad (32)$$

For a reflectivity $(r_2)^2$ of 0.5 or greater, $|\alpha| \geq |\gamma|$. The α terms dominate the γ term in (28), and models that include only a single external cavity reflection are clearly insufficient. Even for $(r_2)^2 = 0.3$, a typical value for uncoated diode facets, $|\alpha| = 0.43|\gamma|$. Equation (32) is independent of the external mirror reflectivity r_3 so even in cases where r_3 is small, it may be inappropriate to use a single external cavity reflection model.

3.2 Steady state mode spectrum

We use our field equation (28) to obtain the steady state solutions of the external cavity laser applicable to the strong regime, briefly review some the fundamental properties of these solutions, and confirm our model gives expected results for non-dispersive cavities; recently steady state characteristics for strong dispersive feedback has also been explored [39]. Assuming the laser field $e_+(t_0, t_1)$ is constant, corresponding to a laser field oscillating at (normalized) frequency $\hat{\omega}$ and given a constant integrated carrier density $\sigma(t_1) = \bar{\sigma}$, we obtain from (28) the steady state condition incorporating infinite external cavity reflections,

$$1 = \left(\alpha + \frac{\gamma \bar{G}}{1 - \bar{G}} \right) \exp(i\hat{\omega}\tau); \tag{33}$$

the frequency-dependent, steady state, round trip gain within the diode is

$$\bar{G} \equiv G(\bar{\sigma}) = r_1 r_2 \exp[i(\hat{\omega} - \beta_c a_0/2)] \exp\left[\frac{1}{2}(1 - i\beta_c)\bar{\sigma}\right]. \tag{34}$$

Combining (33) with (34) and then separating real and imaginary parts, we find the CW mode spectrum for infinite external cavity reflections and the (frequency dependent) carrier density [22, 30, 31]

$$\begin{aligned} \hat{\omega} - \hat{\omega}_{(k)}^{\text{diode}} = & -\frac{1}{2}\beta_c \log \left[1 + \frac{2|\gamma| \cos(\hat{\omega}\tau + \chi_\gamma) - 2|\alpha\gamma| \cos(\Delta\chi) + |\gamma|^2}{1 - 2|\alpha| \cos(\hat{\omega}\tau + \chi_\gamma) + |\alpha|^2} \right] \\ & - \tan^{-1} \left[\frac{|\gamma| \sin(\hat{\omega}\tau + \chi_\gamma) + |\alpha\gamma| \sin(\Delta\chi)}{1 + |\gamma| \cos(\hat{\omega}\tau + \chi_\gamma) - 2|\alpha| \cos(\hat{\omega}\tau + \chi_\alpha) - |\alpha\gamma| \cos(\Delta\chi) + |\alpha|^2} \right], \end{aligned} \tag{35}$$

and

$$\bar{\sigma} - \bar{\sigma}^{\text{diode}} = -\log \left[1 + \frac{2|\gamma| \cos(\hat{\omega}\tau + \chi_\gamma) - 2|\alpha\gamma| \cos(\Delta\chi) + |\gamma|^2}{1 - 2|\alpha| \cos(\hat{\omega}\tau + \chi_\gamma) + |\alpha|^2} \right], \tag{36}$$

where $\chi_\gamma \equiv \arg \gamma$, $\chi_\alpha \equiv \arg \alpha$ and $\Delta\chi \equiv \chi_\alpha - \chi_\gamma$. The steady state spectrum of the solitary diode is given by

$$\hat{\omega}_{(k)}^{\text{diode}} = 2\pi k + \frac{\beta_c}{2} (\sigma^{\text{diode}} + a_0) - \arg(r_1 r_2), \tag{37}$$

for positive integers k , and the steady state carrier density of the solitary diode, $\sigma^{\text{diode}} = -2 \log |r_1 r_2|$, is determined only by cavity losses.

To compare (35) and (36), which take into account an infinite number of external cavity reflections, to the results of the LK model, we again ignore all external cavity reflections beyond the first. Setting $|\alpha| = 0$ in (35) and (36), and expanding the equations to first order in $|\gamma|$, we recover the well-known expressions [12, 40]

$$\hat{\omega} - \hat{\omega}_{(k)}^{\text{diode}} = -|\gamma|(1 + \beta_c^2)^{1/2} \sin(\hat{\omega}\tau + \chi_\gamma + \tan^{-1} \beta_c), \tag{38}$$

$$\bar{\sigma} = -2 \log |r_1 r_2| - 2|\gamma| \cos(\chi_\gamma + \hat{\omega}\tau). \tag{39}$$

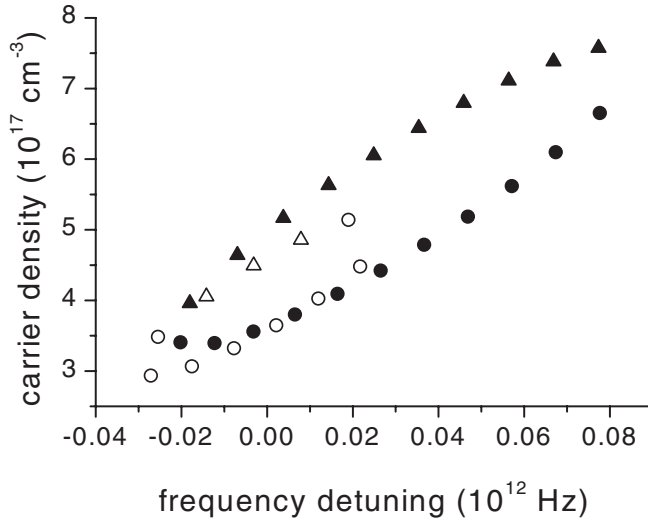


Figure 3. The steady state carrier density versus frequency for the discrete solutions of the steady state transcendental equations resulting from both the LK model (open symbols) and our infinite number of reflections model (filled symbols) for a given k in (37). For our model, the (average) carrier density is $\bar{\sigma}/(2L_g\Gamma a) + N_l$. In both cases, the triangles represent the (unstable) anti-mode solutions and the circles the (nominally stable) mode solutions. We used $\beta_c = 2$, $|r_1|^2 = 0.4$, $|r_2|^2 = 0.4$, $|r_3|^2 = 0.3$ and $L_{ext} = 1$ cm; the index of refraction in the external cavity was taken to be 1.44.

A numerical comparison of (35) and (36) and (38) and (39) is made in figure 3 where we plot the steady state solutions in the $\hat{\omega}$, $\bar{\sigma}$ plane for an example in the strong regime, where we would expect differences between the models to occur. The open symbols represent solutions obtained from (35) and (36), and the closed symbols the LK model. As expected, there are qualitative differences between the solutions. Not only are there approximately double the number of solutions of (35) than there are of (38), but the two ‘islands’ of solutions are not centred about the same point and do not have the same distribution.

As evident from figure 3, the solutions seem to lie on some underlying curve in the $\hat{\omega}$, $\bar{\sigma}$ plane. This ‘locus curve’ has been previously described in detail [22], and is found by taking the squared absolute value of (33); it turns out to be independent of the external cavity round trip time so that τ determines only the number of steady state solutions. Setting $\arg r_3 = \pi$ and again assuming that $\tilde{r}_2 t_2 - \tilde{r}_2 r_2 = 1$ and $\tilde{r}_2 = -r_2$ for r_2 real, we find from (33)

$$0 = |r_1|^2(|r_2|^2 - |r_3|^2) \exp(\bar{\sigma}) + (1 - |r_2 r_3|^2) - 2|r_1 r_2|(1 - |r_3|^2) \cos(\hat{\omega} - \beta_c(\bar{\sigma} - a_0)/2) \exp\left(\frac{1}{2}\bar{\sigma}\right). \tag{40}$$

As discussed in previous work [22], the locus curves are closed for $|r_2| > |r_3|$, resulting in islands of CW modes clustered around the solitary diode laser modes (as in figure 3). They are open for $|r_2| < |r_3|$. An example in each regime is plotted in figure 4, where the solid and dotted lines show the locus curves for external cavity lasers with $|r_2|^2 = 0.4$ and 0.225, respectively, where $|r_1|^2 = 0.4$, $|r_3|^2 = 0.3$ and

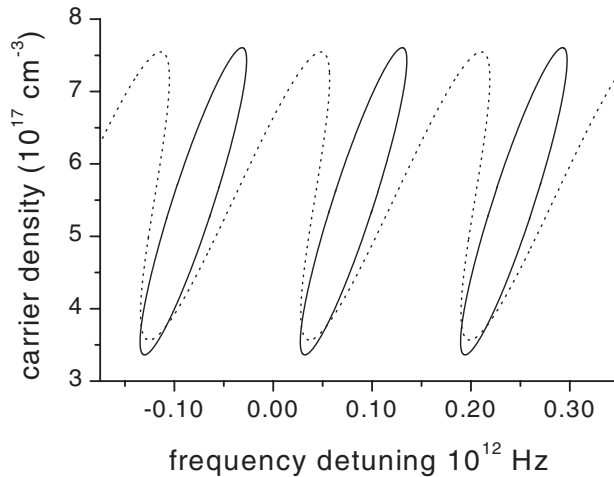


Figure 4. Locus curves of steady state solutions for external cavity semiconductor lasers with $\beta_c = 2$, $|r_1|^2 = 0.4$ and $|r_3|^2 = 0.3$, for $|r_2|^2 = 0.4$ (solid line) and $|r_2|^2 = 0.225$ (dashed line).

$\beta_c = 2$. The tilts of the two curves are determined by the value of the linewidth enhancement factor, β_c [22]: the long axis of the closed curves and the tilted axis of the open curves are given by $\hat{\omega} = \beta_c \bar{\sigma} / 2 + \beta_c a_0 / 2$.

The shape of the locus curves arises from the dominance of either the diode cavity when $|r_2| > |r_3|$, or the combined laser cavity when $|r_2| < |r_3|$; this is revisited in the next subsection, when we choose the mode basis for the decomposition of the field (13) to derive a closed set of dynamical equations. In the limit $|r_3| = 0$, the laser is comprised of only the solitary diode; appropriately, the locus curves collapse to discrete points identified with the Fabry–Pérot modes of the solitary diode laser. As $|r_3|$ increases from zero, the locus curves become islands surrounding these discrete points, becoming larger and larger as the external cavity becomes more and more prominent. In the limit $|r_2| = 0$, such as for an external cavity laser with an ideally antireflection coated diode facet at $z = 0$, the laser again has only a single cavity, a cavity now delimited by the $z = -L_g$ diode facet and the external mirror. The CW solutions and dynamics of this latter special case have been examined earlier in detail for dispersive external cavities [13, 16]. The locus curve is a horizontal line, with equally spaced CW solutions that correspond to the Fabry–Pérot modes of the single cavity laser. As $|r_2|$ increases from zero, the locus curve becomes modulated according to the Fabry–Pérot mode spacing of the diode, and this modulation increases in depth the larger $|r_2|$ becomes. The curve eventually becomes multivalued, as illustrated in figure 4.

Finally, we note that recent theoretical work has argued that any model based on slowly varying envelope approximations (SVEA)—such as this one and indeed all other models cited thus far—are in general not sufficient to describe the physics near the region $|r_2| = |r_3|$. Here there is a so-called ‘metamorphosis’ of the steady state solutions, where the closed curves on the red side of the spectrum merge together to form one large island as $|r_3|$ is increased [41]. This work concludes, therefore, that a correct description of the metamorphosis region then cannot be made with any SVEA model, even if gain dispersion is included [42]. We show in appendix C that

our model is in any case only valid away from $|r_2| = |r_3|$. Thus a purely numerical approach without the SVEA may be required to study the dynamics in this regime.

3.3 Dynamics

In this last subsection, we examine a subset of the dynamical characteristics of the external cavity laser, particularly for strong external cavity feedback where stable operation is both expected and desired for practical devices. Using the (Fourier decomposed) gain medium equations (17) and (18), and an appropriate extension of (25) and (26), we obtain a set of closed equations for the field mode amplitudes and the carrier density. We first apply these equations to assess laser stability via its small signal response. Then, we present numerical solutions of the laser equations for large direct current modulation for strong external feedback. We both identify the main dynamical features of this simulation and show explicitly that the main assumptions required for the multiple scales analysis functions are valid.

Using the Fourier decomposition of the field (13), we combine the boundary conditions (25) and (26) for each mode m with the equations for the diode (17) and (18) to obtain the equation for the m th field mode and the carrier density equation

$$e_{+(m)}(t_1) = \left[\gamma + \alpha \frac{1 - \exp(i2\pi m/\tau_p)G(t_1 - \mu\tau)}{\exp(i2\pi m/\tau_p)G(t_1 - \mu\tau)} \right] \times \frac{G(t_1) \exp(i\hat{\omega}\tau) \exp[i2\pi m(1 + \tau)/\tau_p]}{1 - \exp(i2\pi m/\tau_p)G(t_1)} e_{+(m)}(t_1 - \mu\tau), \quad (41)$$

$$\frac{\partial}{\partial t_1} \sigma(t_1) = j(t_1) - 2(1 - \exp(-\sigma(t_1)/2))(1 + |r_1|^{-2} \exp(-\sigma(t_1)/2)) \sum_m |e_{+(m)}(t_1)|^2, \quad (42)$$

where $G(t_1)$ is the round trip gain, defined by (27). These equations form a closed set for $e_{+(m)}$ and σ , and it is these which we use for the dynamics of the external cavity laser. We choose the parameter τ_p according to the details of the CW mode spectrum. As discussed earlier, for $|r_2| > |r_3|$, the diode cavity dominates the resonance structure, so in this regime we choose the field to be periodic in t_0 with period $\tau_p = 1$, the (normalized) diode round trip time. This approach is only valid when the corresponding locus curve islands, such as those plotted with solid lines in figure 4, do not overlap each other along the frequency axis; this ensures the t_0 and t_1 time scales are properly separated. In appendix C, we calculate the region in $|r_2|$, $|r_3|$ space for which this occurs; the invalid region is indicated by the upper shaded area in figure 5, bounded from above by the upper solid curve and from below by the dotted line indicating $|r_2| = |r_3|$.

For the case where $|r_2| < |r_3|$, the total laser cavity dominates the CW spectrum. We choose $\tau_p = 1 + \tau$ for this region of parameter space. The Fourier decomposition is expressed in terms of extended-cavity laser modes and is valid when the open locus curves are single valued. We calculate also in appendix C the region in $|r_2|$, $|r_3|$ space for which multivaluedness of open locus curves occurs. This is indicated by the lower shaded region in figure 5, bounded from above by $|r_2| = |r_3|$ and from below by the lower solid curve. For the special case where $|r_2| = 0$, and the laser operates within a single extended laser cavity, the field mode equation reduces to a form similar to the field equation obtained earlier for the dispersive single cavity laser [13].

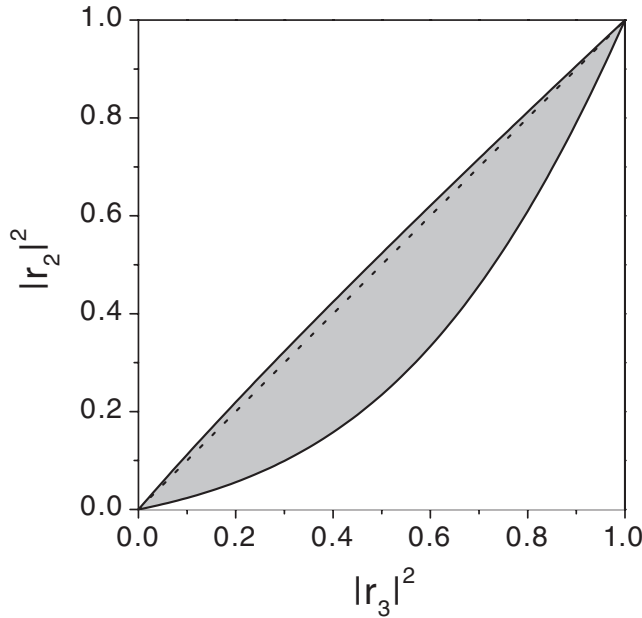


Figure 5. The unshaded regions indicate where the external cavity laser formalism given by (41) and (42) is expected to be valid; we used $\beta_c = 2$.

3.3.1 Small signal response. We assess the stability of the CW modes by applying the dynamical equations (41) and (42) to the study of small-signal response of the laser. We assume the field is oscillating initially at one particular stationary solution, characterized by its steady state frequency $\hat{\omega}$, steady state carrier density $\bar{\sigma}$ and current density $j(t_1) = \bar{j}$; without loss of generality choose the CW solution to be labelled by $m = 0$.

We introduce deviation functions from steady state Δe_+ , $\Delta\sigma$, through

$$e_{+(m=0)}(t_1) = s_+^{1/2} \exp(i\phi)(1 + \Delta e_+(t_1)),$$

$$\sigma(t_1) = \bar{\sigma} + \Delta\sigma(t_1),$$

for arbitrary constant phase ϕ and where the steady state value of the (normalized) photon density s_+ , determined from (42), is

$$s_+ = \frac{1}{2} \frac{\bar{j}}{(1 - \exp(-\bar{\sigma}/2))(1 + |r_1|^{-2} \exp(-\bar{\sigma}/2))}. \tag{43}$$

For small signal response, we need only consider the terms in the field and carrier density equations (41) and (42) that are linear in both Δe_+ and $\Delta\sigma$. The linearized versions of (41) and (42) are

$$\Delta e_+(t_1) - \Delta e_+(t_1 - \mu\tau) = \frac{1}{2} \frac{1 - i\beta_c}{1 - \bar{G}} (\Delta\sigma(t_1) - \alpha \exp(i\hat{\omega}\tau) \Delta\sigma(t_1 - \mu\tau)), \tag{44}$$

$$\frac{\partial}{\partial t_1} \Delta\sigma(t_1) = -\Gamma_1 \Delta\sigma(t_1) - \Gamma_2 (\Delta e_+(t_1) + \Delta e_+^*(t_1)), \tag{45}$$

where we used (27), (33) and (34), and defined the parameters

$$\begin{aligned}\Gamma_1 &= s_+ \exp\left(-\frac{1}{2}\bar{\sigma}\right)\left(1 + 2|r_1|^{-2} \exp\left(-\frac{1}{2}\bar{\sigma}\right) - |r_1|^{-2}\right), \\ \Gamma_2 &= 2s_+\left(1 + |r_1|^{-2} \exp\left(-\frac{1}{2}\bar{\sigma}\right)\right)\left(1 - \exp\left(-\frac{1}{2}\bar{\sigma}\right)\right);\end{aligned}$$

Γ_1 is an effective carrier decay rate and Γ_2 is the linear carrier-field coupling coefficient.

Taking the Laplace transform of the real and imaginary parts of (44), and of (45), we find that non-trivial solutions exist when

$$\begin{aligned}0 &= |\gamma|(s + \Gamma_1)(1 - \exp(-s\mu\tau)) \\ &\quad - \Gamma_2[\cos \hat{\omega}\tau - \beta_c \sin \hat{\omega}\tau - |\gamma| - |\alpha|] \\ &\quad + |\alpha|\Gamma_2 \exp(-s\mu\tau)[1 - (|\gamma| + |\alpha|)(\cos \hat{\omega}\tau + \beta_c \sin \hat{\omega}\tau)],\end{aligned}\quad (46)$$

where s is the complex Laplace variable. We set $\Delta\sigma(t_1 = 0) = 0$ and used (33) to replace \bar{G} . For brevity, we took $\arg r_3 = \pi$, $\tilde{t}_2 t_2 - \tilde{r}_2 r_2 = 1$ and $\tilde{r}_2 = -r_2$ for r_2 real. The stability is assessed for a particular CW frequency $\hat{\omega}$ by finding the complex-valued solutions of s that satisfy this equation, and determining whether or not any of these solutions for s have a positive real part, indicating exponential growth in the linear regime.

By setting $s = s_R + is_I$ for s_R and s_I real, and separating out the real and imaginary parts of (46), we find that there exist CW modes such that $s_I = 0$, and some of these have $s_R > 0$, indicating instability. These CW solutions are known in the literature as ‘anti-modes’ [40], and are indicated in figure 3 by triangles both for our model (filled triangles) and the LK model (open triangles). For strong feedback our model gives the same qualitative results as expected from previous work describing weak feedback [12]. The circles in figure 3 indicate CW solutions without this instability and are known in the literature as ‘modes’ [40]; these are the only candidates for true stable modes. In general, there exist solutions for non-zero s_I and a complete stability determination would need to consider these solutions as well. This has been examined in other work in detail for a single external cavity reflection [12, 40] and for multiple reflections in an interesting recent study [29]. The stability properties for the special case of $r_2 = 0$ for dispersive external cavities has also been considered in detail, where dispersion is seen to play a key role in stability [16].

3.3.2 Large current modulation. Lastly, we turn to an examination of laser dynamics through the numerical solution of (27), (41) and (42). In particular, we consider large modulation of the diode current, typical of non-return-to-zero signals, for a diode with strong external feedback. Our main goals are (i) to identify the major dynamical features of the field intensity and instantaneous frequency response to modulation and (ii) to confirm that the main assertions of the multiple scales analysis are self-consistent. That is, we confirm both that the dynamical variables $e_{+(m)}$, σ are at most of order unity, and that their time dependence is truly a t_1 time dependence: the fastest variations should then occur only on a real time scale of 0 to $(T_g T_n)^{1/2}$ and the functions $e_{+(m)}$, σ should be slowly varying as real time increments by the diode round trip time T_g .

We solve (27), (41) and (42) by implementing a fourth-order Runge–Kutta algorithm to solve the ordinary differential equation (42), where we incorporate

the delay in the field amplitudes and the gain in (41) directly by keeping track of their previous values. For the numerical examples presented below, we choose the laser parameters as described in the caption of figure 3 and listed in table 1 and with CW solutions as plotted in figure 3. We take the initial laser state, from $t_1 = -\mu\tau$ to $t_1 = 0$, to be a CW solution to the ‘mode’ (and not the ‘anti-mode’) closest in frequency to the solitary diode resonance, located at zero frequency detuning in figure 3. Our parameters here are such that $|r_2| > |r_3|$, thus the field is Fourier decomposed according to solitary diode resonances. The solitary diode resonance we consider is the one nearest to 1550 nm and we label the field amplitude corresponding to this resonance by $m = 0$. The initial intensity of this resonance is (43) and the initial intensities of the others ($m \neq 0$)—corresponding in this example to other solitary diode resonances and not to other external cavity modes—are set to zero. The current is held constant throughout the initial phase, but is modulated for times $t_1 > 0$ such that the corresponding steady state field intensity changes by 10 dB.

We plot in figure 6 the case where the current is lowered from its initial value, kept constant for a time, then raised to its initial value—a simple, slow ‘turn-off’, ‘turn-on’ sequence. The normalized intensity is of order unity or smaller throughout, and thus consistent with one set of assumptions of the multiple scales analysis.

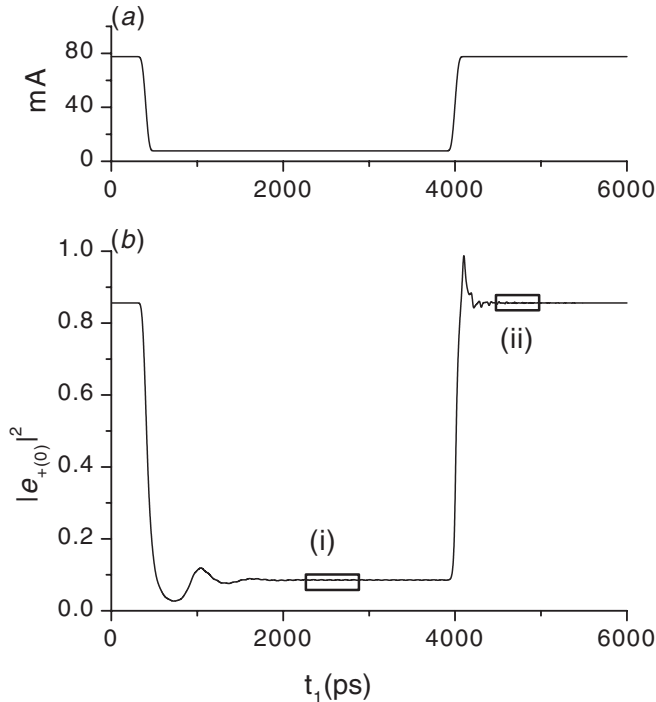


Figure 6. (a) Large signal current modulation and (b) the corresponding response of the normalized field intensity $|e_{\pm(0)}(t_1)|^2$ as a function of t_1 time for a ‘turn-off’, ‘turn-on’ bit sequence. We used the diode parameters listed in table 1 and the other laser parameters outlined in the caption of figure 3. The ‘on’ current level is 80 mA with a 50 injection efficiency assumed. The ‘on’ level corresponds to an intracavity power of approximately 170 mW and the ‘off’ power is 10 dB below this level. The horizontal axis is labelled by the actual time. The boxed sections labelled (i) and (ii) are shown in close-up in figure 7.

After each current change in the sequence, the laser initially undergoes a transient behaviour (relaxation oscillations), eventually settling into a new steady state characterized by that particular current level. Both the decay rate and the dominant oscillation frequency are larger for the ‘turn-on’ transient at the higher current level, than for the ‘turn-off’ transient at the lower current level. This decay rate and frequency dependence on the current is a well-known feature of the relaxation oscillations of semiconductor lasers and is easily found analytically for the small-signal regime using a rate equation model [7, 9]. Upon closer inspection of figure 6, however, it is evident that there is another, more rapid oscillation that is occurring. We show in figure 7 (*a*) and (*b*) close-up views of portions of both the low current and high current transient sections, as labelled in figure 6 by (i) and (ii), respectively. The grid lines in plots (*a*) and (*b*) of figure 7 are located at 96 ps intervals—the round trip time of the external cavity—and in both cases, the fast oscillation that occurs is on this time scale and thus independent of the current. This pulsing behaviour has also been seen for strong feedback in another recent study [29].

To determine whether the field intensity variations are indeed slowly varying on the t_0 time scale, we examine in figure 7(*c*) yet another close up of the ‘turn-on’

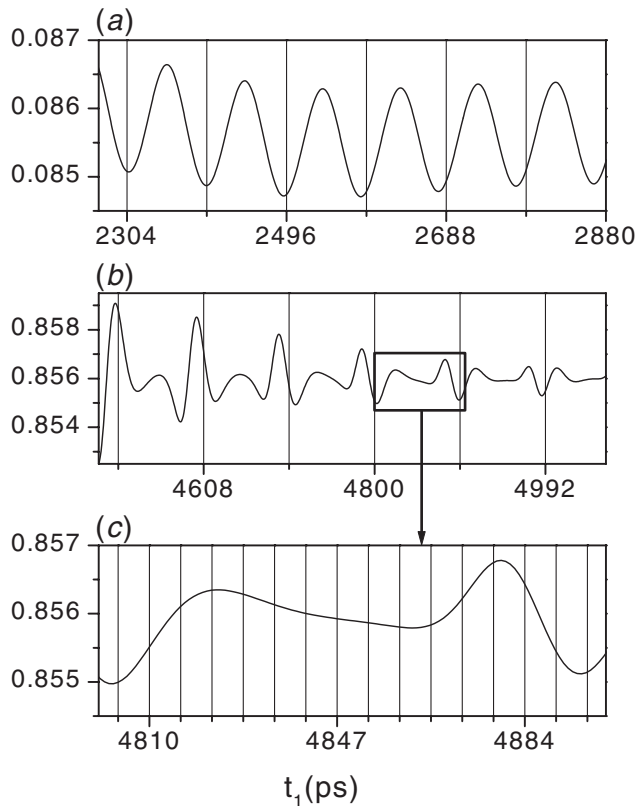


Figure 7. Plots (*a*) and (*b*) depict close-ups of the normalized field intensity time evolution of figure 6, corresponding to the boxed portions of that figure labelled (i) and (ii), respectively. The grids in both (*a*) and (*b*) are located at 96 ps intervals, corresponding to the external cavity round trip time. The boxed portion of (*b*) is itself shown in close-up in plot (*c*). Here the grids indicate 6.17 ps intervals—the round trip time of light within the diode, T_g .

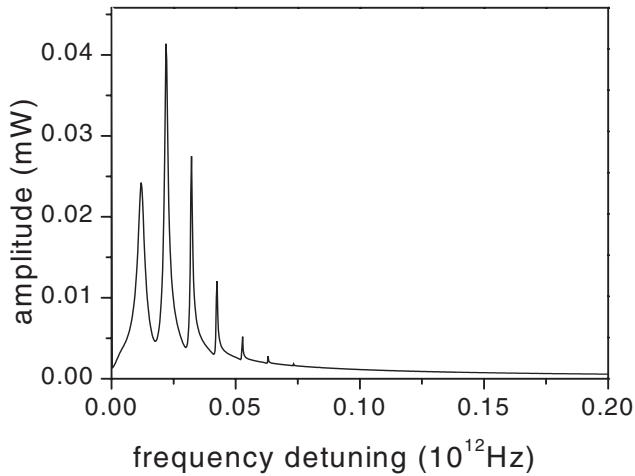


Figure 8. Fourier transform of the tail portion of the ‘turn-on’ transient of figure 6. The large peak at zero frequency detuning is not shown. Note that the other peaks correspond approximately to external cavity resonances, with spacing that is approximately 0.01×10^{12} Hz; there is no peak corresponding to the next solitary diode Fabry–Pérot resonance at 0.16×10^{12} Hz.

transient section, as indicated by the box in figure 7(b) that encloses a single cycle of the faster oscillation. In figure 7(c), the grid lines now indicate intervals of the round trip time of light within the diode, 6.17 ps. Clearly there are no significant variations of the intensity within one round diode trip time, so that this numerical solution of (27), (41) and (42) is consistent with the main assumption of the multiple scales analysis. This is also evident from an examination of the Fourier transform of the tail of the ‘turn-on’ transient, as shown in figure 8. Aside from the very large DC peak at zero frequency detuning that is not shown, there are several smaller peaks, each located approximately 100 ps from each other—indicating the excitation of external cavity resonances—but there is no peak near $1/T_g = 0.162 \times 10^{12}$ Hz, at the next neighbouring solitary diode resonance.

Lastly we consider the laser response to a varied current modulation pattern, with a bit length of 400 ps. The field intensity is plotted in figure 9; not surprisingly, we find a similar relaxation oscillation behaviour as before. In figure 10(a) and (b), we plot the corresponding time evolution of the instantaneous frequency and average carrier density, respectively. The normalized intensity in figure 9 and carrier density in figure 10 are both of order unity or smaller throughout, again indicating consistency with assumptions of the multiple scales analysis. For the limit $|r_2| = 0$, it has been shown in previous work for dispersive external cavities [13] that the instantaneous frequency of the field is proportional to the average carrier density and thus follows its dynamical evolution adiabatically; this can also be deduced from (41). In this numerical example, where parameters are such that we are far from this limit, we see through a comparison of figures 10(a) and (b), that the instantaneous frequency (or more correctly, its time average over T_{ext}) still does follow the dynamics of the carrier density. However, the excitation of external cavity resonances creates significant oscillation in the instantaneous frequency that cause it to deviate from adiabatically following the carrier density time evolution. The carrier

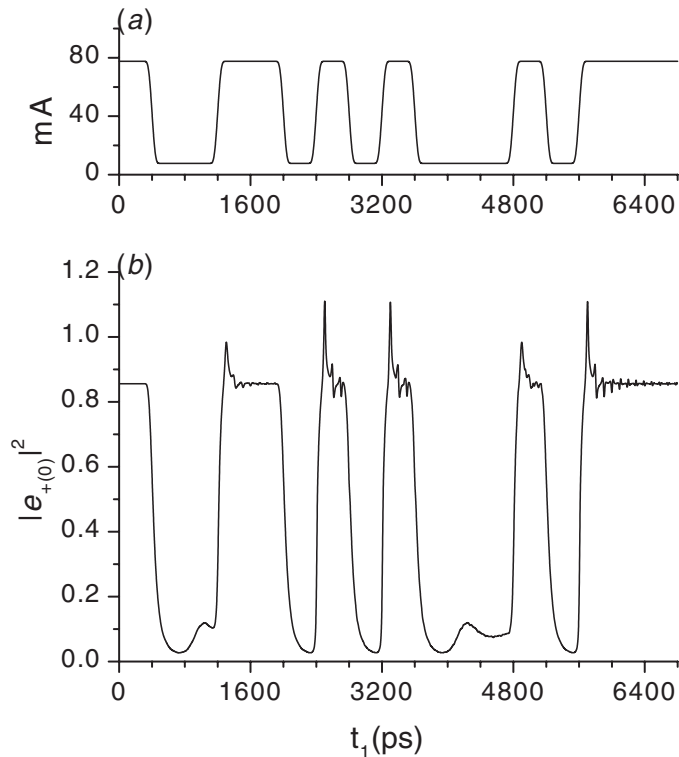


Figure 9. (a) Large signal current modulation and (b) corresponding response of the field intensity $|e_{\pm(0)}(t_1)|^2$ as a function of t_1 time for a bit stream at 2.5 Gbit s^{-1} . Laser parameters are as listed in the caption of figure 6.

density shows only a weak oscillation amplitude on the time scale of the external cavity round trip time.

4. Conclusions

We have presented both a new formalism describing the dynamics of a semiconductor diode and verified its validity through an application to the study of external cavity semiconductor lasers. Beginning with a set of phenomenological travelling wave equations that describe field and carrier dynamics within the diode gain medium, we derived a set of equations which are as accurate, but much simpler in form: we found one ordinary differential equation for the average carrier density in terms of the fields at the diode boundaries and a relation between these boundary fields describing a single pass through the diode. These equations have been derived through a multiple scales analysis in which the main assumption is that the non-radiative recombination time of the carriers is much longer than the round trip time of light within the diode. We have not assumed uniform gain throughout the diode and are thus able to more accurately describe systems in which the non-uniformity in the diode is significant. Since our model involves only fields at the diode boundaries, it is quite straightforward to apply this model in the description of more complicated

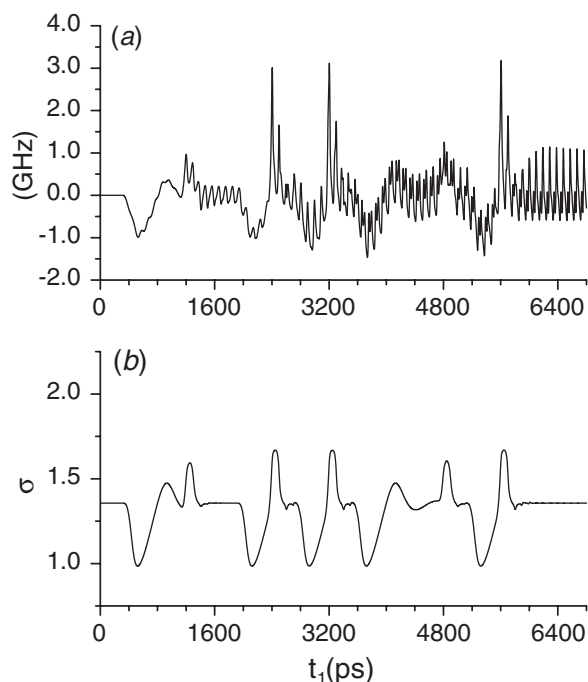


Figure 10. (a) Instantaneous frequency in GHz and (b) (average) carrier density in normalized units, corresponding to the large signal modulation simulation described in figure 9.

systems, wherein a diode is coupled to an external element; one need only supply the boundary conditions at each diode facet.

We have verified our diode model by using it to describe some of the properties of non-dispersive external cavity lasers, concentrating our examples in the strong feedback regime. Applying the boundary conditions appropriate to this system to our diode model, we obtained a set of equations that describe an infinite number of cavity reflections, but that do so with the introduction of only one additional feedback parameter and only one additional delay-term in the field equation. Our approach is equivalent to the more common method of including multiple reflections in strong feedback models, where each external cavity reflection is accounted for explicitly. Further, our model can be rewritten in a form that resembles the standard Lang–Kobayashi field equation in the limit of a single external cavity reflection. After having confirmed that we obtain the expected CW solutions, we examined laser dynamics, both analytically in the small signal limit and numerically for the large signal current modulation of a laser with strong feedback. We used the latter to confirm the self-consistency of the multiple scales analysis and to describe the main dynamical features resulting from current modulation.

Acknowledgments

This work has been supported by the Natural Sciences and Engineering Research Council of Canada.

Appendix A: Notes on carrier density time independence

In this appendix, we rederive standard rate equations describing the time evolution of the fields of both a solitary diode laser and an external cavity laser. Our purpose is to show that in the usual derivations an implicit assumption has been made regarding the time dependence of the carrier density—namely that it is slowly varying—that is not explained and not obviously justifiable. Though a seemingly strong assumption, it does connect to our results in section 2, however, where we find through our more rigorous treatment that to zeroth order, the carrier density is independent of time variable t_0 , associated with the fastest dynamical time scale.

We review first a standard derivation of the field equation describing a solitary diode laser. Beginning with a phenomenological model for the semiconductor diode (and here reverting back to real units), one can obtain a field equation for a solitary diode laser [12]

$$E(t) = g(t)E(t - 1) = g(t) \exp(-d/dt) E(t), \quad (\text{A } 1)$$

by assuming uniform carrier density along the length of the diode, where $E(t)$ is the outgoing field at one of the diode boundaries. The gain resulting from one round trip through the diode is (in our notation)

$$g(t) = \exp\left(\frac{1}{2}(1 - i\beta_c)2\Gamma L_g a(N(t) - N_{\text{th}})\right); \quad (\text{A } 2)$$

the threshold carrier density N_{th} compensates for cavity losses at the diode facets. In their review article [12], van Tartwijk and Lenstra obtain the usual field rate equation by (i) expanding the exponential $\exp(-d/dt)$ to only first order and (ii) approximating $(1 - g^{-1})$ by $\log g$. In fact, one can arrive at the identical rate equation in another way, where the physical consequences of the approximations (i) and (ii) become much more clear. From (A 1), we have

$$\begin{aligned} E(t) &= \exp[\log g(t)] \exp(-d/dt)E(t) \\ &\simeq \exp[\log g(t) - d/dt]E(t), \end{aligned} \quad (\text{A } 3)$$

where in order to obtain the last line, a Baker–Hausdorff expansion must be made and truncated at the first order. This step, as it turns out, is necessary to derive the form of the rate equation that appears in previous work [12], and which we also rederive here. First expanding the exponential function in (A 3) in a Taylor series, we find that by requiring

$$(\log g(t) - d/dt)E(t) = 0$$

we obtain a solution for $E(t)$ that exactly satisfies (A 3) to all orders of the Taylor series. From (A 2), we obtain finally the standard form of the solitary diode equation,

$$\frac{d}{dt}E(t) = \frac{1}{2}(1 - i\beta_c)2\Gamma L_g a(N - N_{\text{th}})E(t). \quad (\text{A } 4)$$

In order to derive (A 4), it was necessary to assume that

$$[\log g(t), d/dt] = 0, \quad (\text{A } 5)$$

where the square brackets denote commutation. Thus it has been implicitly assumed in previous work that the diode round trip gain g and thus the carrier density N are (largely) time independent, though it is not immediately obvious that they necessarily should be.

The usual external cavity diode laser field equation—i.e. the Lang–Kobayashi (LK) equation [24]—is derived from an extension of (A 1) [12]

$$E(t + 1) = g(t)E(t) + g(t)\gamma \exp(i\omega T_{\text{ext}})E(t - T_{\text{ext}}), \tag{A 6}$$

where here only a single external cavity reflection is incorporated, where T_{ext} is the external cavity round trip time, and where an effective feedback parameter had been defined as

$$\gamma = \frac{1 - r_2^2}{r_2} r_3,$$

for real valued reflection coefficients r_2, r_3 ; $g(t)$ is again the round trip gain in the diode (A 2). Transforming (A 6) (without approximation) yields

$$\exp(-\log g(t)) \exp(d/dt) E(t) = E(t) + \gamma \exp(i\omega T_{\text{ext}})E(t - T_{\text{ext}}); \tag{A 7}$$

we call this the ‘precursor’ to the LK equation and it is to this equation that we compare our external cavity laser field equation in section 3. Again we find that it is necessary to make assumption (A 5) to obtain the usual form of the LK equation,

$$\frac{d}{dt} E(t) = \Gamma L_g a(1 - i\beta_c)(N - N_{\text{th}}) E(t) + T_{\text{in}}\gamma \exp(i\omega T_{\text{ext}}) E(t - T_{\text{ext}}).$$

Again, it has been implicitly assumed in previous work that N is (approximately) time independent.

We should note that a similar approximation was also made by Tromborg *et al.* [22]. To derive their (uniform gain) diode model (equation (12)), it was assumed that the gain resulting from a round trip pass through the diode, denoted there by r_L , is slowly varying.

Appendix B: Boundary condition equivalence

We show that the boundary conditions (22) and (23) are equivalent. Shifting (23) in time by T_{ext} , we have

$$E_-(0, t - T_{\text{ext}}) = r_2 E_+(0, t - T_{\text{ext}}) + \frac{\tilde{t}_2 t_2}{\tilde{r}_2} \sum_{n=2}^{\infty} (\tilde{r}_2 r_3 \exp(i\omega T_{\text{ext}}))^{n-1} E_+(0, t - nT_{\text{ext}}). \tag{B 1}$$

Subtracting (B 1) times $\tilde{r}_2 r_3 \exp(i\omega T_{\text{ext}})$ from (23) gives (22).

Appendix C: Region of validity

In this appendix, we determine the region of parameter space where we expect the equations describing the dynamics of the external cavity laser (41) and (42) to be valid. We base our validity determination on the characteristics of the locus curves of the steady state solutions (40) for values of $|r_2|^2$ and $|r_3|^2$ between zero and one. For closed locus curve solutions, occurring when $|r_2|^2 > |r_3|^2$, we expect our formalism to be valid only when successive locus curve ‘islands’, such as those plotted in figure 4, do not overlap with each other in frequency $\hat{\omega}$. This then ensures that the t_0 time dependence, characterized by (13) with $\tau_p = 1$, does not overlap with the t_1 time dependence of the Fourier components of the field. The overlapping occurs when the distance given by the projection of a single island onto the normalized frequency axis exceeds a value of 2π . We find this distance by determining at what frequencies the derivative $d\bar{\sigma}/d\hat{\omega}$ is infinite. For open locus curve solutions, occurring when $|r_2|^2 < |r_3|^2$, we choose $\tau_p = 1 + \tau$, and the field is decomposed into extended cavity modes. This is expected to be valid only when the locus curves are not multivalued, that is, when $d\bar{\sigma}/d\hat{\omega}$ is finite for all $\hat{\omega}$.

We find $d\bar{\sigma}/d\hat{\omega}$ by implicitly differentiating the locus curve (40) with respect to $\hat{\omega}$. It is infinite only when $|r_2|$, $|r_3|$ and β_c satisfy

$$0 \leq \frac{|r_3|^2(1 - |r_2|^2)^2}{|r_2|^2(1 - |r_3|^2)^2} \leq 1 + \beta_c^2. \quad (\text{C1})$$

This condition is always satisfied for the closed locus curve solutions (which are inherently multivalued) and satisfied for open curves only for parameters such that

$$|r_2|^4|r_3|^2 - \left(1 + |r_3|^4 + \beta_c^2(1 - |r_3|^2)^2\right)|r_2|^2 + |r_3|^2 \leq 0. \quad (\text{C2})$$

The region where the description (41) and (42) is not valid for $|r_2|^2 < |r_3|^2$ is indicated by the lower shaded area of figure 5, which is bounded from above by $|r_2|^2 = |r_3|^2$ (dotted line) and bounded from below by the line given by equality in (C2) (lower solid line).

We now seek the region for which (41) and (42) are valid for closed locus curves ($|r_2|^2 > |r_3|^2$). This occurs when the frequency range of the closed locus curves—i.e. the distance between the frequency locations at which $d\bar{\sigma}/d\hat{\omega}$ is infinite—is less than 2π , so that successive islands do not overlap. We find the boundary between the valid and invalid region to be

$$|r_2|^4 - \frac{(1 + \beta_c^2)(1 + |r_3|^4) - 2\beta_c^2(1 - c)|r_3|^2}{(1 + c\beta_c^2)|r_3|^2} |r_2|^2 + 1 = 0, \quad (\text{C3})$$

where we have defined

$$c = \left(\frac{\exp(2\pi/\beta_c) + 1}{\exp(2\pi/\beta_c) - 1} \right)^2.$$

The upper shaded region of figure 5, bounded from below by $|r_2|^2 = |r_3|^2$ (dotted line) and from above by (C 3) (upper solid line), then indicates the region of invalidity of (41) and (42) for $|r_2|^2 > |r_3|^2$.

References

- [1] P.S. Bhatia, G.R. Welch and M.O. Scully, *Opt. Commun.* **189** 321 (2001).
- [2] D.T. Cassidy and M.J. Hamp, *J. Mod. Opt.* **46** 1071 (1999).
- [3] P.A. Morton, V. Mizrahi, R. Tanbun-Ek, *et al.*, *Appl. Phys. Lett.* **64** 2634 (1994).
- [4] J.S. Lawrence and D.M. Kane, *IEEE J. Quantum Electron.* **38** 185 (2002).
- [5] F.N. Timofeev, I.S. Kostko, P. Bayvel, *et al.*, *Electron. Lett.* **35** 1737 (1999).
- [6] H. Bissessur, C. Caraglia, B. Thedrz, *et al.*, *IEEE Photonics Technol. Lett.* **11** 1304 (1999).
- [7] G.P. Agrawal and N.K. Dutta, *Semiconductor Lasers*, 2nd ed. (Van Nostrand Reinhold, New York, 1993).
- [8] H. Ghafouri-Shiraz, *Fundamentals of Laser Diode Amplifiers* (J. Wiley, New York, 1996).
- [9] K. Petermann, *Laser Diode Modulation and Noise* (Kluwer Academic Publishers, Boston, 1988).
- [10] L.M. Zhang and J.E. Carroll, *IEEE J. Quantum Electron.* **28** 604 (1992).
- [11] G.C. Dente and M.L. Tilton, *IEEE J. Quantum Electron.* **34** 325 (1998).
- [12] G.H.M. van Tartwijk and D. Lenstra, *Quantum Semiclass. Opt.* **7** 87 (1995).
- [13] L. Ramunno and J.E. Sipe, *IEEE J. Quantum Electron.* **36** 1299 (2000).
- [14] L. Ramunno and J.E. Sipe, *IEEE J. Quantum Electron.* **35** 624 (1999).
- [15] M.W. Pan, B.P. Shi and G.R. Gray, *Opt. Lett.* **22** 166 (1997).
- [16] L. Ramunno and J.E. Sipe, *Phys. Rev. A* **66** 033817 (2002).
- [17] A.P.A. Fischer, O.K. Andersen, M. Yousefi, *et al.*, *IEEE J. Quantum Electron.* **36** 375 (2000).
- [18] M. Yousefi and D. Lenstra, *IEEE J. Quantum Electron.* **36** 970 (1999).
- [19] F. Di Teodoro, E. Cerboneschi, D. Hennequin, *et al.*, *Quantum Semiclass. Opt.* **9** 867 (1997).
- [20] A.P.A. Fischer, M. Yousefi, D. Lenstra, *et al.*, *Phys. Rev. Lett.* **32** 023901 (2004).
- [21] R.K. Dodd, J.C. Eibeck, J.D. Gibbon, *et al.*, *Solitons and Nonlinear Wave Equations* (Academic Press, Toronto, 1982).
- [22] B. Tromborg, H. Olesen, X. Pan, *et al.*, *IEEE J. Quantum Electron.* **QE-23** 1875 (1987).
- [23] T.W. Carr, D. Pieroux and P. Mandel, *Phys. Rev. A* **63** 033817 (2001).
- [24] R. Lang and K. Kobayashi, *IEEE J. Quantum Electron.* **QE-16** 347 (1980).
- [25] R.W. Tkach and R.A. Chraplyvy, *J. Lightwave Technol.* **LT-4** 1655 (1986).
- [26] A.V.T. Cartaxo and J.A.P. Morgado, *Fiber Integrated Opt.* **20** 295 (2001).
- [27] L.N. Langlely, K.A. Shore and J. Mørk, *Opt. Lett.* **19** 2137 (1994).
- [28] P.S. Spencer and K.A. Shore, *Quantum Semiclass. Opt.* **9** 819 (1997).
- [29] S.G. Abdulrhmann, M. Ahmed, T. Okamoto, *et al.*, *IEEE J. Select. Topics Quantum Electron.* **9** 1265 (2003).
- [30] P. Zorabedian, *IEEE J. Quantum Electron.* **30** 1542 (1994).
- [31] B. Tromborg, J. Mørk and V. Velichansky, *Quantum Semiclass. Opt.* **9** 831 (1997).
- [32] P. Vankwikelberge, G. Morthier and R. Baets, *IEEE J. Quantum Electron.* **26** 1728 (1990).
- [33] D. Marcuse, *IEEE J. Quantum Electron.* **QE-19** 63 (1983).
- [34] M. Schell, A.G. Weber, E.H. Böttcher, *et al.*, *IEEE J. Quantum Electron.* **27** 402 (1991).
- [35] P. Brosson, *J. Lightwave Technol.* **12** 49 (1994).
- [36] B. Tromborg, H.E. Lassen, H. Olesen, *et al.*, *IEEE Photonics Technol. Lett.* **4** 985 (1992).
- [37] O. Hess and T. Kuhn, *Prog. Quantum Electron.* **20** 85 (1996).

- [38] G. Morthier and P. Vankwikelberge, *Handbook of Distributed Feedback Laser Diodes* (Artech House, Inc., Boston, 1997).
- [39] A. Naumenko, P. Besnard, N. Loiko, *et al.*, IEEE J. Quantum Electron. **39** 1216 (2003).
- [40] J. Mørk, B. Tromborg and J. Mark, IEEE J. Quantum Electron. **28** 93 (1992).
- [41] A.A. Duarte and H.G. Solari, Phys. Rev. A **58** 614 (1998).
- [42] A.A. Duarte and H.G. Solari, Phys. Rev. A **64** 033803 (2001).